Laser Amplification in Strongly Magnetized Plasma

Matthew R. Edwards,[1,*] Yuan Shi,[2,3,4,†] Julia M. Mikhailova,[1,‡] and Nathaniel J. Fisch[2,3,§]
[1]Department of Mechanical and Aerospace Engineering, Princeton University, Princeton, New Jersey 08544, USA
[2]Department of Astrophysical Sciences, Princeton University, Princeton, New Jersey 08544, USA
[3]Princeton Plasma Physics Laboratory, Princeton, New Jersey 08543, USA
[4]Lawrence Livermore National Laboratory, Livermore, California 94550, USA

(Received 14 November 2018; revised manuscript received 28 May 2019; published 9 July 2019)

We consider backscattering of laser pulses in strongly magnetized plasma mediated by kinetic magnetohydrodynamic waves. Magnetized low-frequency (MLF) scattering, which can occur when the external magnetic field is neither perpendicular nor parallel to the laser propagation direction, provides an instability growth rate higher than Raman scattering and a frequency downshift comparable to Brillouin scattering. In addition to the high growth rate, which allows smaller plasmas, and the 0.1%–2% frequency downshift, which permits a wide range of pump sources, MLF scattering is an ideal candidate for amplification because the process supports an exceptionally large bandwidth, which particle-in-cell simulations show produces ultrashort durations. Under some conditions, MLF scattering also becomes the dominant spontaneous backscatter instability, with implications for magnetized laser-confinement experiments.

DOI: 10.1103/PhysRevLett.123.025001

Laser-driven magnetic field generation has produced kilotesla (10 MG) field strengths with coil-type targets [1–7], far beyond what can be achieved with permanent magnets. These magnetic fields, and the 10 to 100 kT (100 MG to 1 GG) strengths envisioned for future experiments [8], may enhance inertial confinement fusion (ICF) [9–11], accelerate particles more effectively [12,13], and provide new capabilities for high-energy-density physics and laboratory astrophysics [14,15]. Strong magnetic fields also open a new regime of laser-plasma interaction (LPI) physics [16], holding both the promise of useful new nonlinearities and the risk of damaging scattering in implosion-type experiments.

A problem of particular importance in LPI physics is the scattering of laser beams from electron or ion waves. This can be either a deleterious effect, e.g., loss of energy from stimulated scattering or cross-beam energy transfer [17–19], or a beneficial instability useful for the construction of ultra-high-power plasma-based parametric amplifiers [20]. Plasma components in high-power lasers avoid damage thresholds set by solid-state optics, allowing extraordinarily high-peak-power lasers to be envisioned without prohibitive beam diameters. Parametric plasma amplification, where a plasma wave compresses a long-duration high-energy pump into a short lower-frequency high-power seed, is a key component of proposed plasma-based laser amplifier chains. Current plasma amplifiers are based on two established mechanisms: stimulated Raman scattering (SRS) [21–34], where the Langmuir wave provides high growth rates but large frequency downshifts, or stimulated Brillouin scattering (SBS) [35–49], where the ion-acoustic wave mediates the interaction, giving lower growth rates but allowing higher-efficiency energy extraction and smaller frequency separations between seed and pump. Initial work has examined how magnetic fields modify Raman and Brillouin scattering [50–52] or extended Raman scattering to the upper hybrid wave [53,54], though simulations have been restricted to external fields exactly parallel or perpendicular to the pump-laser propagation vector ($\mathbf{k}$).

Here we demonstrate that the rich physics of strongly magnetized plasma offers a third distinct mechanism for plasma amplification: scattering from the kinetic extensions of magnetohydrodynamic (MHD) waves, which exhibits an instability growth rate comparable to or higher than Raman scattering with a much smaller frequency downshift and appears when the applied magnetic field is neither perpendicular nor parallel to the laser propagation vector. Since this interaction disappears in unmagnetized plasma and lacks an analogue in nonionized media, we refer to it here as magnetized low-frequency (MLF) scattering for the mediating plasma response. MLF scattering is promising for amplification because (1) the growth rate is larger than Raman scattering, allowing rescaling for shorter interaction duration and plasma size, (2) the frequency of the plasma response, and thus the frequency difference between the two lasers, is small, reducing the technical difficulty of creating a suitable seed and leading to higher efficiencies, (3) the interaction bandwidth is wide, supporting short-duration pulse generation, and (4), group velocity dispersion in the magnetized medium is large, permitting self-compression of broad-bandwidth amplified pulses to

ultrashort duration. In this Letter we use particle-in-cell (PIC) simulations supported by an analytic theory to examine MLF scattering of laser pulses in magnetized plasma.

Consider spontaneous backscattering of a laser (frequency ω_0) normally incident on an underdense ($\omega_e < \omega_0$) semi-infinite homogeneous plasma. For negligible magnetic field magnitude (B_0), spontaneous Raman and Brillouin scattering may both occur. However, a much more complex picture for backscattering emerges when the electron cyclotron frequency ($\Omega_e = eB/m_e c$) is not negligible compared to ω_0, and $\mathbf{B}_0$ and $\mathbf{k}$ are neither exactly parallel nor perpendicular. Figure 1 presents backscattered spectra for $0.01 < \Omega_e/\omega_0 < 10$ and $\theta = \langle \mathbf{B}_0, \mathbf{k} \rangle = 75°$, calculated using one-dimensional (1D) three-velocity-component (3V) PIC simulations (EPOCH [55]). With resolution $\lambda/\Delta x = 50$ and 40 particles/cell, a linearly polarized laser ($\mathbf{E} \perp \mathbf{B}_0$) with normalized field strength $a_0 = eE/m_e\omega_0 c = 0.01$ and wavelength $\lambda = 1$ μm ($I = 1.38 \times 10^{14}$ W/cm^2) strikes an electron-proton plasma ($N = n_e/n_c = 0.01$ where n_c is the critical density, temperature $T_e = T_i = 1$ eV). The spectral energy distributions are provided for 300 simulations at varied B_0 after 2 ps. Backscattering for $0 < B_0 < 100$ T is invariant with B_0 on this scale. At $B_0 = 100$ T the spectrum is dominated by Raman scattering at $\omega = \omega_0 - \omega_e$ and Brillouin scattering at $\omega = \omega_0 - c_s k \approx \omega_0$, where c_s is the sound speed.

Above $B_0 = 1000$ T ($\Omega_e/\omega_0 > 0.1$) the spectral energy distribution changes substantially. When Ω_e is comparable to ω_e (here $\omega_e/\omega_0 = 0.1$), Raman scattering becomes scattering from the upper-hybrid (UH) wave, where $\omega_{\mathrm{UH}} = \sqrt{\omega_e^2 + \Omega_e^2}$ for $\theta \approx 90°$; the Raman-UH line curves towards lower frequencies for larger magnetic fields. The increased scattering from the UH line near 5 kT can be called two-magnon decay, which occurs when the incident field decays into two upper-hybrid waves and is analogous to two-plasmon decay in unmagnetized plasma. The transition to the upper-hybrid wave moderately improves laser amplification [53,54], but the most striking signature in Fig. 1 is the strong scattering that appears between $0.5 < \Omega_e/\omega_0 < 1.2$ at $\omega/\omega_0 \approx 0.99$. As described below, this scattering comes from kinetic MHD waves, i.e., MLF scattering, and is notable for both its large strength and small downshift from the pump frequency.

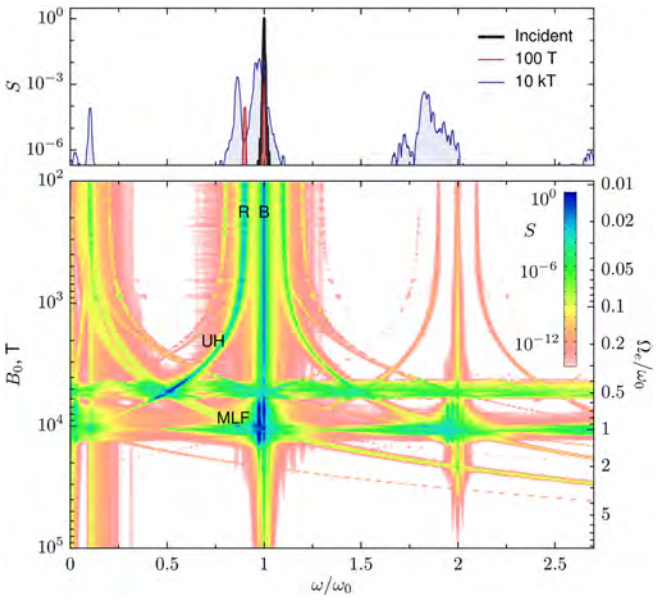

FIG. 1. Spectral energy distribution of light backscattered from magnetized plasma ($N = 0.01$, $T_e = T_i = 1$ eV, $m_i/m_e = 1836$) in PIC simulations. The magnetic field B_0 varies between 100 T and 10 kT at $\theta = 75°$. The spectra are measured in vacuum ($\omega/\omega_0 = k/k_0$). Color indicates spectral energy density logarithmically. (Top) Spectra of the incident and reflected light. $\lambda/\Delta x = 50$ and 40 particles/cell.

Figure 2(a) provides the backscattered spectral energy distribution at $B_0 = 8100$ T ($\Omega_e/\omega_0 = 0.75$), where MLF scattering dominates for $0 \le \theta \le 90°$. This scattering is strongest for θ around 80° and disappears at $\theta = 90°$. When $\theta \to 0$, MLF scattering asymptotes to Raman and Brillouin scattering. The downshift frequency dependence on angle follows the fluid theory (dashed lines) and is relatively small for the large angles where the scattering is most powerful.

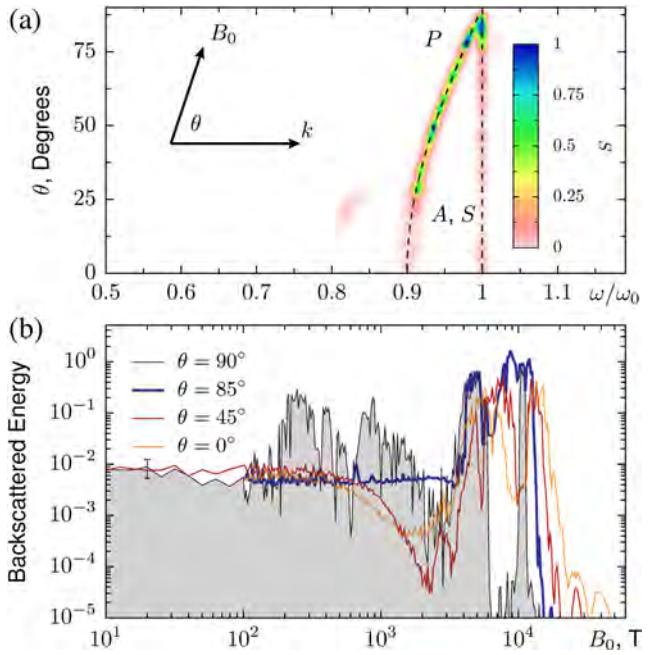

FIG. 2. (a) Backscattered spectra from magnetized electron-proton plasma ($N = 0.01$, $T_e = T_i = 1$ eV) against θ at $\Omega_e/\omega_0 = 0.75$ ($B_0 = 8100$ T), illustrating dependence of MLF scattering on angle. Dashed lines show analytic predictions for the kinetic fast wave (P), Alfvén wave (A) and slow wave (S). (b) Time-averaged backscattered energy over incident energy for selected angles. The reflected power ratio can briefly climb above 1 due to amplitude fluctuations in the scattered radiation. The error bar indicates uncertainty from time variation of the reflected signal. $\lambda/\Delta x = 50$ and 40 particles/cell.

Strong magnetic fields also substantially affect the total scattered energy. As Fig. 2(b) illustrates, though previous work found suppressed backscattering for moderate applied fields (e.g., <50 T [52]), backscattering is dramatically enhanced when ω_0 and Ω_e are comparable. Due primarily to MLF scattering, the strongest signal occurs at intermediate θ when $\Omega_e \approx \omega_0$. Interestingly, at even higher B_0 ($\Omega_e \gg \omega_0$), electron responses are suppressed and there is little backscattering for all θ; although the required fields are large, this regime may ultimately prove useful for scattering suppression in confinement experiments.

Since earlier analysis focused on $\theta = 0$, 90°, this instability has not previously been captured, but recent theoretical advances provide a route to understanding scattering mechanisms at oblique magnetic field angles [56,57]. The coupling coefficient for these modes computed from warm-fluid theory [58] is

$$\Gamma = \sum_s \frac{Z_s \omega_s^2 (\Theta^s + \Phi^s)}{4 M_s (u_1 u_2 u_3)^{1/2}}, \tag{1}$$

where $Z_s = e_s/e$ and $M_s = m_s/m_e$ are the normalized charge and mass of species s, and $\omega_s = \sqrt{4\pi n_s e_s^2/m_s}$. In the denominator, u is the energy coefficient of a participating wave, such that the averaged wave energy is $u|\mathbf{E}|^2/8\pi$. In the numerator, Θ^s is the normalized electromagnetic scattering strength, which comes from the $\mathbf{d}^j(\partial_j \mathbf{A}_i)\mathbf{J}^i$ term in the third-order interaction Lagrangian and equals the sum of six permutations of $\Theta^s_{1,\bar{2},\bar{3}}$, where $\Theta^s_{i,jl} = (c\mathbf{k}_i \cdot \mathbf{f}_{s,j})(\mathbf{e}_i \cdot \mathbf{f}_{s,l})/\omega_j$ for wave frequency ω, propagation vector $\mathbf{k}$, and unit electric polarization vector $\mathbf{e}$ where $\mathbf{f}_s = \hat{\mathbb{F}}_s \mathbf{e}$, and $\hat{\mathbb{F}}_s$ is related to the linear susceptibility by $\chi_s = -\omega_s^2 \hat{\mathbb{F}}_s/\omega^2$. The thermal scattering Φ^s is usually subdominate because $\Phi^s \propto u_s^2/c^2$, where u_s is the thermal speed. For counterpropagating lasers interacting via MLF waves, exact growth rates and frequencies are found from the above general formula by (1) matching resonance conditions using the wave dispersion relations, (2) computing the polarization vectors of the eigenmodes, and (3) finding the linear susceptibility in a magnetized warm-fluid plasma. Analytic expressions valid for all angles and not-well-separated frequencies—the case for the MLF modes—are unwieldy, precluding inclusion here. Instead, we plot the wave dispersion relations and the growth rates calculated from Eq. (1) in Fig. 3.

There are three MLF branches in two-species plasmas. In the low-k limit these branches are the MHD waves, specifically when $\omega_e < \Omega_e$, the Langmuir-type fast (compressional) wave (P), the shear Alfvén wave (A), and the slow (sound) wave (S). In the high-k limit, these wave branches continue beyond the validity of MHD, becoming the kinetic extensions of the MHD waves. The three branches cross and hybridize in a variety of ways depending on θ, the species mass ratio, and the ratio of c_s and the Alfvén speed v_A [59].

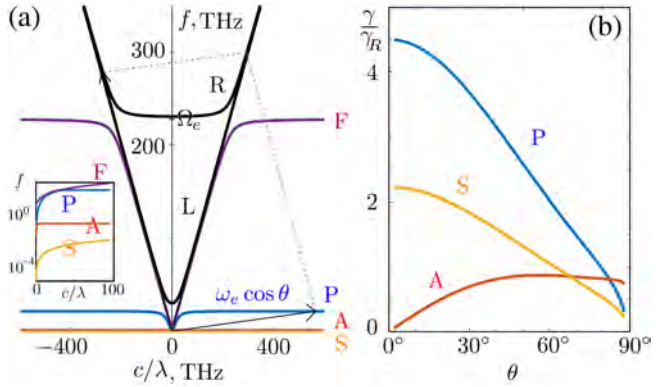

FIG. 3. (a) The dispersion relations in magnetized plasma for right-handed elliptically polarized light (R, black), the upper-hybrid wave (F, purple) and the MLF waves, which are the high-k asymptotes of the fast wave (P, blue), the Alfvén wave (A, red), and the slow wave (S, orange). In the high-k limit, the MLF waves have negligible group velocity. For $\omega \gtrsim \Omega_e \gg \omega_e$, the dispersion relation of right-handed (R) elliptically polarized lasers is strongly modified (upper black curve), producing large group velocity dispersion. Strong interactions only occur between R polarized lasers. Inset: Logarithmic scale. (b) Analytic MLF-scattering growth rates compared to that for unmagnetized Raman scattering (γ_R) at the conditions in Fig. 2(a). For $\theta = \langle \mathbf{B}_0, \mathbf{k} \rangle \sim 75°$, mediation by each MLF branch has a comparable growth rate, so the different branches contribute together over a large bandwidth. At these parameters the upper-hybrid wave cannot resonantly interact.

When $\Omega_e \gg \omega_e$ and $v_A \gg c_s$, the upper branch is the Langmuir wave, the lower branch is the ion-cyclotron wave, and the bottom branch is the sound wave for parallel wave propagation. When the propagation is nearly perpendicular to $\mathbf{B}_0$, the upper branch is the lower-hybrid wave, and the frequencies of the other two branches, both proportional to $\cos\theta$, approach zero. At general angles, MLF waves have intermediate frequencies and mixed characteristics. For the large wave vectors relevant for stimulated laser scattering the MLF waves are almost longitudinal and group velocities are negligible [Fig. 3(a)].

When ω_0 lies slightly above Ω_e and $\Omega_e \gg \omega_e$, the right-handed (R) elliptically polarized component of the laser is strongly coupled with electron cyclotron motion, strongly modifying the wave dispersion relation [Fig. 3(a), black]. If $\mathbf{k}$ is parallel or perpendicular to $\mathbf{B}_0$, laser absorption by a single electron is forbidden by energy-momentum conservation, but at oblique angles resonant absorption is possible. The resonantly driven electron-cyclotron motion produces an enhanced diamagnetic field. The electron gyrofrequency decreases in this screened magnetic field. Upon deexcitation, the electrons emit an electromagnetic wave with slightly downshifted frequency, and the magnetic field relaxes to its original strength. This scattering process involves both the electrons and magnetic field, rather than resonances provided by quasiparticles. MLF scattering therefore has a larger cross section than both

Raman scattering, which relies on plasmons, and Brillouin scattering, dependent on phonons. At oblique angles, the MLF-mediated growth rates [Fig. 3(b)] are comparable to or larger than the Raman growth rate in an unmagnetized plasma of the same density.

To examine whether the MLF instability is useful for laser amplification we conducted PIC simulations with a counterpropagating pump-seed geometry, allowing us to avoid warm-fluid-model restrictions, check for competing instabilities and unanticipated nonlinear or kinetic effects, and capture physics beyond three-wave coupling, which is important because multiple MLF branches may contribute to a single interaction. Figure 4 compares SRS, SBS, and stimulated MLF scattering. Each case had the same plasma density ($N = 0.01$), plasma length ($L = 175\ \mu\text{m} = 175\lambda$), and pump amplitude ($a_0 = 0.007$). The initial seed duration was 400 fs and the pump was uniform in time. In the magnetized case, both the seed and pump were elliptically polarized with Stokes parameters $Q = 0.78I_0$, $U = 0.49I_0$, $V = 0.38I_0$ for propagation through magnetized plasma. Linear polarization was used for the unmagnetized case. Simulations were conducted at varied seed wavelength,

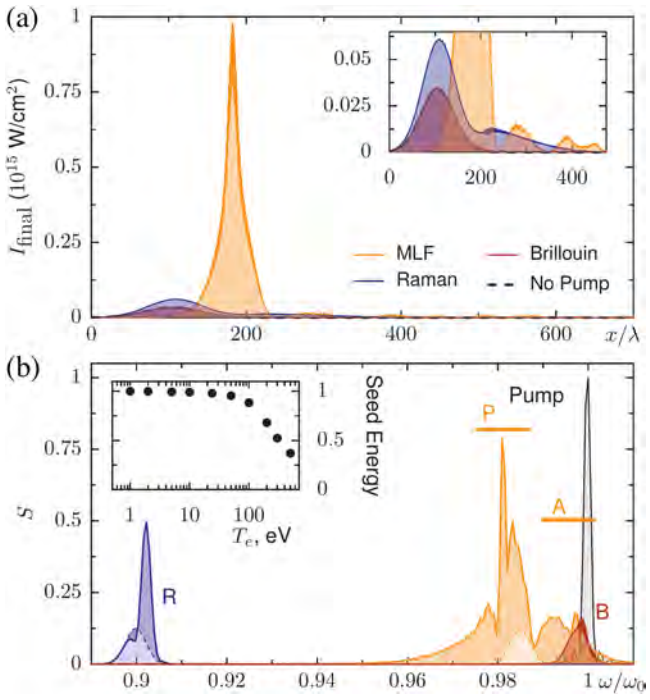

FIG. 4. PIC simulations of amplification via stimulated Raman (R), Brillouin (B), and MLF (P, A) scattering. (a) Seed after interaction in plasma ($N = 0.01$, $L = 175\lambda$) with a counterpropagating pump ($a_0 = 0.007$, $\lambda = 1\ \mu$m, $I = 6.7 \times 10^{13}$ W/cm^2). (b) Spectra of the initial (dashed) and amplified (solid) seed pulses for each mechanism, together with the pump. $\lambda/\Delta x = 150$, 200 particles/cell, $T_e = T_i = 1$ eV and $m_i/m_e = 1836$. For MLF, $B_0 = 9900$ T and $\theta = 80°$. The initial seed intensities are half the pump intensity. Inset: variation in normalized seed final energy with T_e for MLF mechanism.

with the strongest response for each mechanism presented. In comparison to SRS and SBS, MLF scattering exhibits a higher growth rate and broader spectral response; the amplified pulse has more energy and a shorter duration. To isolate the new physics, we neglected collisions and chose low temperatures to reduce Landau damping. Wave damping significantly reduces coupling strength only for $T_e > 200$ eV [Fig. 4(b) inset], leaving a noncollisional regime for MLF scattering.

Figure 4(b) shows that MLF scattering produces a broad bandwidth compared to Raman or Brillouin scattering, which results from both the high growth rate of each MLF branch and the simultaneous contribution of multiple branches with overlapping spectra to a single interaction. For these parameters, a particularly strong interaction is mediated by the Langmuir-type fast wave with frequency $\sim\omega_e \cos\theta$ (Fig. 3, blue), which corresponds to the response near $\omega/\omega_0 \approx 0.98$ in Fig. 4(b) (orange, P). Additionally, the Alfvén branch with frequency $\sim\sqrt{\Omega_e\Omega_i}\cos\theta$ provides strong coupling (Fig. 3, red) and is responsible for the peak near $\omega/\omega_0 \approx 0.995$ in Fig. 4(b) (orange, A). The slow MHD branch would also have a large coupling coefficient, but the three-wave resonance conditions cannot be satisfied at these specific parameters. In short, PIC calculations confirm that MLF-mediated scattering produces a large growth rate over a wide bandwidth with a small frequency downshift, supporting the efficient generation of ultrashort high-power pulses.

Increased group-velocity dispersion provides one further advantage in magnetized plasma. Pulse compression occurs because the seed pulse depletes the pump beam; only the leading edge of the seed is amplified, so the seed will be shorter if pump energy can be extracted more quickly. Some additional self-compression can arise from dispersion for chirped pulses. For Raman amplification, shorter pulse duration requires higher plasma density (increasing plasma frequency), but this increases detrimental secondary effects, including forward scattering, collisional damping, and the modulational instability. Chirping the seed pulse [60] was proposed to avoid these effects. Since lower-frequency electromagnetic waves propagate at smaller group velocity, a chirped seed pulse with $\partial\omega/\partial t > 0$ will self-contract if the plasma ends when the seed pulse is shortest. The equation governing the pulse envelope b can be written $(\partial_t + v_g\partial_x + i\tau\partial_t^2)b = 0$ in the absence of a pump and the modulational instability. The group velocity dispersion coefficient is $\tau = -\frac{1}{2}Gv_g$, where $G = \partial^2 k/\partial\omega^2$. Under the strongly magnetized conditions in Fig. 4, τ is almost three orders of magnitude larger than its unmagnetized value and, consequently, a chirped seed self-compresses within a shorter plasma length. Additionally, the frequency downshift of MLF scattering is more sensitive to B_0 and θ than plasma density, relaxing requirements on plasma homogeneity for resonance condition matching. The highest fields currently achieved—produced by direct laser irradiation

of solid targets—are stationary and uniform over ~1 ps and ~10 μm [61,62]. Although better uniformity is likely required for pulse compression, the large bandwidth of MLF may tolerate fluctuations in field strength or angle. A strong gradient in a diverging magnetic field could also be applied instead of density gradients [63] or pump chirp matching [64] for precursor suppression. The interplay between field gradients and transverse filamentation instabilities may further affect the process, a question which remains to be investigated.

Although the B_0 required to see MLF scattering is high, 5–10 kT (50–100 MG) fields are not far beyond current state-of-the-art capabilities. Furthermore, scaling to longer wavelengths reduces absolute field requirements because three-wave coupling is governed by Ω_e/ω_0. For CO_2 lasers ($\lambda = 10.6$ μm), only 500 T is required. Signatures of enhanced spontaneous scattering may appear in experiments without counterpropagating beams, clarifying mechanisms of potential damage to laser facilities.

In conclusion, we have demonstrated that kinetic MHD waves will strongly backscatter a laser propagating in plasma at an oblique angle to a sufficiently strong magnetic field. This powerful backscattering is potentially useful for laser amplification because the instability growth occurs more quickly than for Raman amplification at the same density, and the frequency downshift is comparable to that of Brillouin amplification. Additionally, substantial spectral broadening is observed in PIC simulations, supporting amplified pulses with ultrashort duration. The frequency downshift is small enough and the spectral response sufficiently broad to prepare the pump and seed from the same source. MLF-wave-mediated instabilities represent a new class of backscattering mechanisms, distinct from both Raman and Brillouin scattering, which may be critical in high-intensity laser experiments with strong applied or self-generated magnetic fields.

This work was supported by NNSA Grant No. DENA0002948, AFOSR Grant No. FA9550-15-1-0391, NSF Grant No. PHY 1506372, and DOE Grant No. DE-SC0017907. Computing support for this work came from the High Performance Computing Center at Princeton University. The EPOCH code was developed as part of the UK EPSRC 300 360 funded Project No. EP/G054940/1. Y. S. is in part supported by the Lawrence Fellowship through LLNL-LDRD Program from Project No. 19-ERD-038 under the auspices of the U.S. Department of Energy by Lawrence Livermore National Laboratory under Contract No. DE-AC52-07NA27344.

M. R. E. and Y. S. contributed equally to this work.

*mredward@princeton.edu
†shi9@llnl.gov
‡j.mikhailova@princeton.edu
§fisch@princeton.edu

[1] J. Knauer *et al.*, Compressing magnetic fields with high-energy lasers, Phys. Plasmas **17**, 056318 (2010).
[2] H. Yoneda, T. Namiki, A. Nishida, R. Kodama, Y. Sakawa, Y. Kuramitsu, T. Morita, K. Nishio, and T. Ide, Strong Compression of a Magnetic Field with a Laser-Accelerated Foil, Phys. Rev. Lett. **109**, 125004 (2012).
[3] S. Fujioka *et al.*, Kilotesla magnetic field due to a capacitor-coil target driven by high power laser, Sci. Rep. **3**, 1170 (2013).
[4] B. Zhu *et al.*, Strong magnetic fields generated with a simple open-ended coil irradiated by high power laser pulses, Appl. Phys. Lett. **107**, 261903 (2015).
[5] K. Law *et al.*, Direct measurement of kilo-tesla level magnetic field generated with laser-driven capacitor-coil target by proton deflectometry, Appl. Phys. Lett. **108**, 091104 (2016).
[6] J. Santos *et al.*, Laser-driven platform for generation and characterization of strong quasi-static magnetic fields, New J. Phys. **17**, 083051 (2015).
[7] Z. Zhang *et al.*, Generation of strong magnetic fields with a laser-driven coil, High Power Laser Sci. Eng. **6**, e38 (2018).
[8] Ph. Korneev, E. d'Humières, and V. Tikhonchuk, Gigagauss-scale quasistatic magnetic field generation in a snail-shaped target, Phys. Rev. E **91**, 043107 (2015).
[9] O. V. Gotchev, P. Y. Chang, J. P. Knauer, D. D. Meyerhofer, O. Polomarov, J. Frenje, C. K. Li, M. J.-E. Manuel, R. D. Petrasso, J. R. Rygg, F. H. Séguin, and R. Betti, Laser-Driven Magnetic-Flux Compression in High-Energy-Density Plasmas, Phys. Rev. Lett. **103**, 215004 (2009).
[10] P. Y. Chang, G. Fiksel, M. Hohenberger, J. P. Knauer, R. Betti, F. J. Marshall, D. D. Meyerhofer, F. H. Séguin, and R. D. Petrasso, Fusion Yield Enhancement in Magnetized Laser-Driven Implosions, Phys. Rev. Lett. **107**, 035006 (2011).
[11] S. A. Slutz and R. A. Vesey, High-Gain Magnetized Inertial Fusion, Phys. Rev. Lett. **108**, 025003 (2012).
[12] F. Pérez, A. Kemp, L. Divol, C. D. Chen, and P. K. Patel, Deflection of MeV Electrons by Self-Generated Magnetic Fields in Intense Laser-Solid Interactions, Phys. Rev. Lett. **111**, 245001 (2013).
[13] A. Arefiev, T. Toncian, and G. Fiksel, Enhanced proton acceleration in an applied longitudinal magnetic field, New J. Phys. **18**, 105011 (2016).
[14] K. Matsuo *et al.*, Magnetohydrodynamics of laser-produced high-energy-density plasma in a strong external magnetic field, Phys. Rev. E **95**, 053204 (2017).
[15] J. Santos *et al.*, Laser-driven strong magnetostatic fields with applications to charged beam transport and magnetized high energy-density physics, Phys. Plasmas **25**, 056705 (2018).
[16] Y. Shi, H. Qin, and N. J. Fisch, Laser-plasma interactions in magnetized environment, Phys. Plasmas **25**, 055706 (2018).
[17] D. H. Froula *et al.*, Increasing Hydrodynamic Efficiency by Reducing Cross-Beam Energy Transfer in Direct-Drive-Implosion Experiments, Phys. Rev. Lett. **108**, 125003 (2012).
[18] J. Moody *et al.*, Multistep redirection by cross-beam power transfer of ultrahigh-power lasers in a plasma, Nat. Phys. **8**, 344 (2012).
[19] J. A. Marozas, M. Hohenberger, M. J. Rosenberg, D. Turnbull, T. J. B. Collins, P. B. Radha, P. W. McKenty,

J. D. Zuegel, F. J. Marshall, S. P. Regan, T. C. Sangster, W. Seka, E. M. Campbell, V. N. Goncharov, M. W. Bowers, J.-M. G. Di Nicola, G. Erbert, B. J. MacGowan, L. J. Pelz, and S. T. Yang, First Observation of Cross-Beam Energy Transfer Mitigation for Direct-Drive Inertial Confinement Fusion Implosions Using Wavelength Detuning at the National Ignition Facility, Phys. Rev. Lett. **120**, 085001 (2018).

[20] V. M. Malkin, G. Shvets, and N. J. Fisch, Fast Compression of Laser Beams to Highly Overcritical Powers, Phys. Rev. Lett. **82**, 4448 (1999).

[21] V. M. Malkin, G. Shvets, and N. J. Fisch, Ultra-powerful compact amplifiers for short laser pulses, Phys. Plasmas **7**, 2232 (2000).

[22] Y. Ping, W. Cheng, S. Suckewer, D. S. Clark, and N. J. Fisch, Amplification of Ultrashort Laser Pulses by a Resonant Raman Scheme in a Gas-Jet Plasma, Phys. Rev. Lett. **92**, 175007 (2004).

[23] W. Cheng, Y. Avitzour, Y. Ping, S. Suckewer, N. J. Fisch, M. S. Hur, and J. S. Wurtele, Reaching the Nonlinear Regime of Raman Amplification of Ultrashort Laser Pulses, Phys. Rev. Lett. **94**, 045003 (2005).

[24] J. Ren, S. Li, A. Morozov, S. Suckewer, N. A. Yampolsky, V. M. Malkin, and N. J. Fisch, A compact double-pass Raman backscattering amplifier/compressor, Phys. Plasmas **15**, 056702 (2008).

[25] N. A. Yampolsky, N. J. Fisch, V. M. Malkin, E. J. Valeo, R. Lindberg, J. Wurtele, J. Ren, S. Li, A. Morozov, and S. Suckewer, Demonstration of detuning and wavebreaking effects on Raman amplification efficiency in plasma, Phys. Plasmas **15**, 113104 (2008).

[26] Y. Ping *et al.*, Development of a nanosecond-laser-pumped Raman amplifier for short laser pulses in plasma, Phys. Plasmas **16**, 123113 (2009).

[27] G. Vieux *et al.*, Chirped pulse Raman amplification in plasma, New J. Phys. **13**, 063042 (2011).

[28] R. M. G. M. Trines, F. Fiúza, R. Bingham, R. A. Fonseca, L. O. Silva, R. A. Cairns, and P. A. Norreys, Production of Picosecond, Kilojoule, and Petawatt Laser Pulses via Raman Amplification of Nanosecond Pulses, Phys. Rev. Lett. **107**, 105002 (2011).

[29] D. Turnbull, S. Li, A. Morozov, and S. Suckewer, Possible origins of a time-resolved frequency shift in Raman plasma amplifiers, Phys. Plasmas **19**, 073103 (2012).

[30] S. Depierreux, V. Yahia, C. Goyon, G. Loisel, P.-E. Masson-Laborde, N. Borisenko, A. Orekhov, O. Rosmej, T. Rienecker, and C. Labaune, Laser light triggers increased Raman amplification in the regime of nonlinear Landau damping, Nat. Commun. **5**, 4158 (2014).

[31] Z. Toroker, V. M. Malkin, and N. J. Fisch, Backward Raman amplification in the Langmuir wavebreaking regime, Phys. Plasmas **21**, 113110 (2014).

[32] G. Lehmann and K. Spatschek, Non-filamentated ultra-intense and ultra-short pulse fronts in three-dimensional Raman seed amplification, Phys. Plasmas **21**, 053101 (2014).

[33] M. R. Edwards, Z. Toroker, J. M. Mikhailova, and N. J. Fisch, The efficiency of Raman amplification in the wave-breaking regime, Phys. Plasmas **22**, 074501 (2015).

[34] M. R. Edwards, K. Qu, J. M. Mikhailova, and N. J. Fisch, Beam cleaning of an incoherent laser via plasma Raman amplification, Phys. Plasmas **24**, 103110 (2017).

[35] A. Andreev, C. Riconda, V. Tikhonchuk, and S. Weber, Short light pulse amplification and compression by stimulated Brillouin scattering in plasmas in the strong coupling regime, Phys. Plasmas **13**, 053110 (2006).

[36] L. Lancia *et al.*, Experimental Evidence of Short Light Pulse Amplification Using Strong-Coupling Stimulated Brillouin Scattering in the Pump Depletion Regime, Phys. Rev. Lett. **104**, 025001 (2010).

[37] G. Lehmann, F. Schluck, and K. H. Spatschek, Regions for Brillouin seed pulse growth in relativistic laser-plasma interaction, Phys. Plasmas **19**, 093120 (2012).

[38] G. Lehmann and K. Spatschek, Nonlinear Brillouin amplification of finite-duration seeds in the strong coupling regime, Phys. Plasmas **20**, 073112 (2013).

[39] S. Weber, C. Riconda, L. Lancia, J.-R. Marquès, G. A. Mourou, and J. Fuchs, Amplification of Ultrashort Laser Pulses by Brillouin Backscattering in Plasmas, Phys. Rev. Lett. **111**, 055004 (2013).

[40] C. Riconda, S. Weber, L. Lancia, J.-R. Marques, G. A. Mourou, and J. Fuchs, Spectral characteristics of ultra-short laser pulses in plasma amplifiers, Phys. Plasmas **20**, 083115 (2013).

[41] E. Guillaume *et al.*, Demonstration of laser pulse amplification by stimulated Brillouin scattering, High Power Laser Sci. Eng. **2**, e33 (2014).

[42] G. Lehmann and K. Spatschek, Temperature dependence of seed pulse amplitude and density grating in Brillouin amplification, Phys. Plasmas **23**, 023107 (2016).

[43] L. Lancia, A. Giribono, L. Vassura, M. Chiaramello, C. Riconda, S. Weber, A. Castan, A. Chatelain, A. Frank, T. Gangolf, M. N. Quinn, J. Fuchs, and J.-R. Marquès, Signatures of the Self-Similar Regime of Strongly Coupled Stimulated Brillouin Scattering for Efficient Short Laser Pulse Amplification, Phys. Rev. Lett. **116**, 075001 (2016).

[44] M. Chiaramello, F. Amiranoff, C. Riconda, and S. Weber, Role of Frequency Chirp and Energy Flow Directionality in the Strong Coupling Regime of Brillouin-Based Plasma Amplification, Phys. Rev. Lett. **117**, 235003 (2016).

[45] M. R. Edwards, N. J. Fisch, and J. M. Mikhailova, Strongly Enhanced Stimulated Brillouin Backscattering in an Electron-Positron Plasma, Phys. Rev. Lett. **116**, 015004 (2016).

[46] Q. Jia, I. Barth, M. R. Edwards, J. M. Mikhailova, and N. J. Fisch, Distinguishing Raman from strongly coupled Brillouin amplification for short pulses, Phys. Plasmas **23**, 053118 (2016).

[47] M. R. Edwards, Q. Jia, J. M. Mikhailova, and N. J. Fisch, Short-pulse amplification by strongly-coupled stimulated Brillouin scattering, Phys. Plasmas **23**, 083122 (2016).

[48] M. R. Edwards, J. M. Mikhailova, and N. J. Fisch, X-ray amplification by stimulated Brillouin scattering, Phys. Rev. E **96**, 023209 (2017).

[49] J.-R. Marquès *et al.*, Joule-Level High-Efficiency Energy Transfer to Subpicosecond Laser Pulses by a Plasma-Based Amplifier, Phys. Rev. X **9**, 021008 (2019).

[50] L. Yin, B. Albright, H. Rose, D. Montgomery, J. Kline, R. Kirkwood, P. Michel, K. Bowers, and B. Bergen, Self-organized coherent bursts of stimulated Raman scattering and speckle interaction in multi-speckled laser beams, Phys. Plasmas **20**, 012702 (2013).

[51] A. Paknezhad, Effect of DC-magnetic field on the growth rate of Raman backscattering of X-mode laser in magnetized collisional plasma, Laser Part. Beams **34**, 80 (2016).

[52] B. Winjum, F. Tsung, and W. Mori, Mitigation of stimulated Raman scattering in the kinetic regime by external magnetic fields, Phys. Rev. E **98**, 043208 (2018).

[53] Y. Shi, H. Qin, and N. J. Fisch, Laser-pulse compression using magnetized plasmas, Phys. Rev. E **95**, 023211 (2017).

[54] Q. Jia, Y. Shi, H. Qin, and N. J. Fisch, Kinetic simulations of laser parametric amplification in magnetized plasmas, Phys. Plasmas **24**, 093103 (2017).

[55] T. D. Arber, K. Bennett, C. S. Brady, A. Lawrence-Douglas, M. G. Ramsay, N. J. Sircombe, P. Gillies, R. G. Evans, H. Schmitz, A. R. Bell, and C. P. Ridgers, Contemporary particle-in-cell approach to laser-plasma modelling, Plasma Phys. Controlled Fusion **57**, 113001 (2015).

[56] Y. Shi, H. Qin, and N. J. Fisch, Three-wave scattering in magnetized plasmas: From cold fluid to quantized Lagrangian, Phys. Rev. E **96**, 023204 (2017).

[57] Y. Shi, Three-wave interactions in magnetized warm-fluid plasmas: General theory with evaluable coupling coefficient, arXiv:1903.02745.

[58] Although the standard nomenclature is "kinetic MHD waves," they can be analytically treated with fluid models: A kinetic treatment is unnecessary and MHD is insufficient.

[59] T. E. Stringer, Low-frequency waves in an unbounded plasma, J. Nucl. Energy C **5**, 89 (1963).

[60] Z. Toroker, V. M. Malkin, and N. J. Fisch, Seed Laser Chirping for Enhanced Backward Raman Amplification in Plasmas, Phys. Rev. Lett. **109**, 085003 (2012).

[61] M. Borghesi, A. J. MacKinnon, A. R. Bell, R. Gaillard, and O. Willi, Megagauss Magnetic Field Generation and Plasma Jet Formation on Solid Targets Irradiated by an Ultraintense Picosecond Laser Pulse, Phys. Rev. Lett. **81**, 112 (1998).

[62] G. Chatterjee, P. K. Singh, A. P. L. Robinson, D. Blackman, N. Booth, O. Culfa, R. J. Dance, L. A. Gizzi, R. J. Gray, J. S. Green, P. Koester, G. R. Kumar, L. Labate, A. D. Lad, K. L. Lancaster, J. Pasley, N. C. Woolsey, and P. P. Rajeev, Micron-scale mapping of megagauss magnetic fields using optical polarimetry to probe hot electron transport in petawatt-class laser-solid interactions, Sci. Rep. **7**, 8347 (2017).

[63] Yu. A. Tsidulko, V. M. Malkin, and N. J. Fisch, Suppression of Superluminous Precursors in High-Power Backward Raman Amplifiers, Phys. Rev. Lett. **88**, 235004 (2002).

[64] V. M. Malkin, G. Shvets, and N. J. Fisch, Detuned Raman Amplification of Short Laser Pulses in Plasma, Phys. Rev. Lett. **84**, 1208 (2000).